JEM Journal of Experimental Medicine

BRIEF DEFINITIVE REPORT

Trav15-dv6 family *Tcrd* rearrangements diversify the *Tcra* repertoire

Danielle J. Dauphars[1], Ariana Mihai[1], Liuyang Wang[2], Yuan Zhuang[1], and Michael S. Krangel[1]

The *Tcra* repertoire is generated by multiple rounds of V_α-J_α rearrangement. However, *Tcrd* recombination precedes *Tcra* recombination within the complex *Tcra-Tcrd* locus. Here, by ablating *Tcrd* recombination, we report that *Tcrd* rearrangement broadens primary V_α use to diversify the *Tcra* repertoire in mice. We reveal that use of Trav15-dv6 family V gene segments in *Tcrd* recombination imparts diversity in the *Tcra* repertoire by instigating use of central and distal V_α segments. Moreover, disruption of the regions containing these genes and their *cis*-regulatory elements identifies the Trav15-dv6 family as being responsible for driving central and distal V_α recombinations beyond their roles as substrates for *Tcrd* recombination. Our study demonstrates an indispensable role for *Tcrd* recombination in general, and the Trav15-dv6 family in particular, in the generation of a combinatorially diverse *Tcra* repertoire.

Introduction

TCR and BCR repertoires rely on combinatorial diversity imparted by V(D)J recombination of variable (V), diversity (D), and joining (J) gene segments at their respective antigen receptor (AgR) loci (Schatz and Ji, 2011). The lymphocyte-specific recombination-activating gene (RAG) proteins mediate double-stranded DNA breaks at recognition sites, called "recombination signal sequences" (RSSs), flanking the V, D, and J segments of the AgR loci. These breaks are then modified, and the segments are ligated via nonhomologous end joining and spliced to a constant gene segment (C) to make AgR chain transcripts (Schatz and Ji, 2011; Helmink and Sleckman, 2012). RAG binding at AgR loci is primarily restricted to recombination centers (RCs), chromatin regions characterized by highly accessible clusters of J (and sometimes D) segments (Ji et al., 2010; Schatz and Ji, 2011). In order for V-to-(D)J recombination to occur, V segments must be brought into proximity of the RC (Jhunjhunwala et al., 2009; Lin et al., 2018). This process is tightly regulated, and ordered recombinations are integral to successful generation of a diverse TCR repertoire. *Tcrd*, *Tcrg*, and *Tcrb* rearrangements occur at the $CD4^-CD8^-$ (double-negative [DN]) stage of thymocyte development (Capone et al., 1998). Subsequently, *Tcra* undergoes V_α-to-J_α recombination at the $CD4^+CD8^+$ (double-positive [DP]) stage (Petrie et al., 1995).

Because *Tcra* recombinations involve only V_α and J_α segments, *Tcra* is capable of undergoing multiple rounds of rearrangement to generate a functional, in-frame TCRα chain (Petrie et al., 1993; Wang et al., 1998). The first V-to-J_α rearrangement is referred to as the "primary rearrangement," and all subsequent *Tcra* recombination events are referred to as "secondary rearrangements" (Carico and Krangel, 2015). Primary *Tcra* rearrangements typically involve the most V_α-proximal J_α segments (Thompson et al., 1990), which constitute the initial *Tcra* RC. High-throughput sequencing (HTS) of the *Tcra* repertoire demonstrates that early V_α rearrangements are broadly distributed, including the proximal half of the V_α array as well as substantial central and distal V_α contributions. Secondary rearrangements proceed to more distal V_α and J_α segments over time, with the *Tcra* RC continually retargeted in stepwise fashion to more distal J_α segments following each round of V_α-J_α rearrangement (Hawwari and Krangel, 2007; Ji et al., 2010; Schatz and Ji, 2011; Carico et al., 2017). Notably, in a mouse in which all thymocytes have a knock-in of the rearrangement *Trav17-Traj57* (Buch et al., 2002), the progression of secondary rearrangements was found to be tightly constrained, with each round of secondary recombinations limited to the most proximal of the remaining V_α and J_α segments (Carico et al., 2017). Because the combinatorial space occupied by secondary rearrangements downstream of a single primary rearrangement is narrow, repertoire diversity must depend on broad use of V_α segments in primary rearrangements.

The *Tcra-Tcrd* locus displays a unique structure among AgR loci, wherein D_δ and J_δ gene segments are nested between the V_α

[1]Department of Immunology, Duke University Medical Center, Durham, NC; [2]Department of Molecular Genetics and Microbiology, Duke University Medical Center, Durham, NC.

Correspondence to Michael S. Krangel: krang001@mc.duke.edu.

and J_α gene segments, and V_δ segments are interspersed among the V_α segments in both mouse and man (Fig. 1 A; Glusman et al., 2001; Carico and Krangel, 2015). Intriguingly, many of the central and distal V_α segments used in primary and early secondary rearrangements were found to be immediately upstream of segments that can be used as *Tcrd* recombination substrates (Carico et al., 2017). Most cells that express αβTCRs first undergo *Tcrd* rearrangement on at least one allele (Livak et al., 1995; Nakajima et al., 1995; Sleckman et al., 1998; Shih et al., 2012). These truncating recombinations delete V_α segments located between the recombined V_δ and D_δ segments before *Tcra* rearrangement begins. Therefore, *Tcrd* rearrangement could bias *Tcra* recombination toward the use of more distal V_α segments for primary rearrangements than would be observed on alleles that do not recombine *Tcrd*.

Most deletional V-to-DJ_δ recombination events in mice involve D_δ-proximal V_δ segments, thereby leaving most of the V_α array intact (Chen et al., 2015; Zhao et al., 2016). One V_δ family, Trav15-dv6, accounts for most of the distal *Tcrd* rearrangements that do occur. As Trav15-dv6 rearrangements would truncate the V_α array and change the starting point for primary *Tcra* rearrangements, we hypothesized that Trav15-dv6 rearrangement may be fundamental to combinatorial diversity of the *Tcra* repertoire.

In a mouse model of altered chromatin looping at the *Tcra-Tcrd* locus, V-to-DJ_δ recombination was found to be skewed toward rearrangement of the proximal *Trdv2-2* and *Trdv3* gene segments, with concomitant reductions in rearrangements to distal V_δ segments (Chen et al., 2015; Zhao et al., 2016). *Tcra* rearrangements were also found to be less diverse, consistent with a role for *Tcrd* recombination in *Tcra* repertoire formation. However, because the primary effect of mutation in this model is on chromatin looping, it remains unclear whether the observed *Tcra* repertoire phenotype may be a direct consequence of this structural change as opposed to an indirect consequence of altered *Tcrd* rearrangements.

Here, we employed an HTS approach (Carico et al., 2017) to determine the impact of *Tcrd* recombination on the *Tcra* repertoire in DP thymocytes using several novel mouse models. In primary mouse thymocytes incapable of *Tcrd* rearrangement, we observed a dramatic contraction in *Tcra* repertoire diversity, directly implicating *Tcrd* recombination in *Tcra* repertoire formation. Moreover, deletion of *Trav15d-1-dv6d-1* or *Trav15-1-dv6-1* revealed the rearrangement of these V_δ segments to be particularly important in targeting primary *Tcra* rearrangements to the distal and central portions of the V_α array, respectively. Finally, we provide evidence that Trav15-dv6 or flanking elements may also have a direct effect on the *Tcra* repertoire by facilitating secondary V_α-to-J_α rearrangement events.

Results and discussion

Tcrd recombination diversifies *Tcra* repertoire

To directly assess the impact of *Tcrd* recombination on the *Tcra* repertoire, we sought a mouse strain incapable of *Tcrd* recombination. In this regard, the C_δ-KO mouse undergoes normal *Tcrd* rearrangement (Itohara et al., 1993), and the E_δ-KO mouse has only a partial defect (Monroe et al., 1999). Therefore, we generated a novel line of mice lacking a 24-kb region containing the D_δ and J_δ segments (Figs. 1 A and S1 A). The resulting mouse, D_δ and J_δ deficient (DJD), ablates V-to-DJ_δ rearrangement and γδT cells, with otherwise normal thymocyte development (Fig. S1, B–D).

Preselection DP thymocytes from DJD mice and their WT littermates were subjected to 5′ rapid amplification of cDNA ends (RACE) and *Tcra* sequencing. Unique clones were analyzed to determine the frequencies of V-to-J_α rearrangements. As previously reported (Carico et al., 2017), in WT thymocytes, we found the *Tcra* repertoire to be diverse (Fig. 1 B, left panel; and Fig. S2 A). Proximal J_α segments frequently rearranged with proximal, central, and distal V_α segments. Secondary rearrangements occurred mostly along two distinct diagonals (Fig. S2 B). The major diagonal started with proximal and central V-to-proximal J_α primary rearrangements, followed by secondary rearrangements through the central and distal V_α and J_α segments. The minor diagonal arose from distal V-to-proximal J_α primary rearrangements. In DJD thymocytes, absent *Tcrd* recombination, we observed restricted V_α use; proximal J_α segments recombined almost exclusively with the most proximal V_α segments (Fig. 1 B, right panel). This reduction in diversity of V_α use in early rearrangements with proximal J_α segments depressed the diversity of secondary rearrangements, with a notable loss in the use of distal V_α segments, even in recombinations with central and distal J_α segments. The major diagonal was constrained and shifted toward more proximal V_α segments along its entire length; the minor diagonal was largely depleted of unique clones.

Previous work described the progression of secondary rearrangements emanating from a single primary recombination as proceeding ∼1.33 V_α segments per J_α (Carico et al., 2017). According to our hypothesis, DJD thymocytes should be depleted of V-J_α combinations resulting from primary rearrangements distal to the most proximal Trav15-dv6 family member, *Trav15-2-dv6-2*, as well as any secondary rearrangements that occur as a consequence of those primary rearrangements. To assess this, we overlaid a step-function diagonal ($4V_\alpha$:$3J_\alpha$, corresponding to 1.33 V_α per J_α) over the DJD–WT difference map, with its origin just distal to *Trav15-2-dv6-2* (Fig. 1 C). The step-function diagonal predicts almost exactly the region of depletion of the combinatorial *Tcra* repertoire in DJD thymocytes. In WT thymocytes, the region above the diagonal accounts for 43% of the repertoire; in DJD thymocytes, it accounts for 22% (Fig. 1, B and C; $P < 0.0001$ by χ^2 test with Yates's correction). However, this is a substantial underestimate of the impact on some distal V_α rearrangements. Prior work demonstrated that the SD of the V_α distribution used with any J_α gradually increases from proximal to distal across the J_α array (Carico et al., 2017). Because this increase is not accounted for by the step-function diagonal, we would expect representation of the most distal V_α-distal J_α combinations to persist, although at reduced frequencies, in the region above the diagonal in DJD thymocytes (compare Fig. 1 B, right panel, with Fig. 1 C). This effect should not impact quantification along the minor diagonal; accordingly, rearrangements in this region account for 7.7% of the repertoire in WT but only 2% in DJD

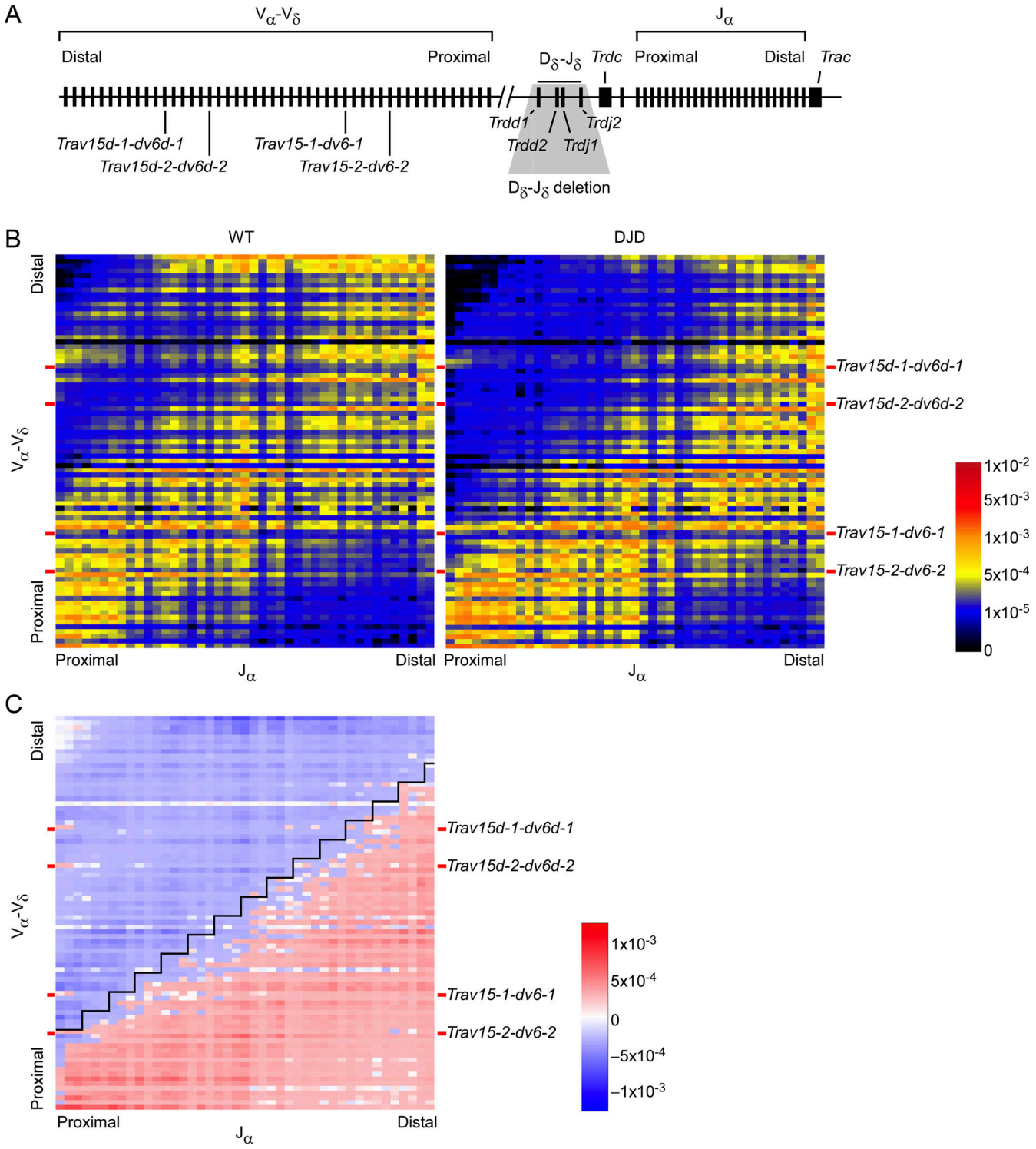

Figure 1. ***Tcrd* recombination diversifies *Tcra* repertoire. (A)** Schematic of the *Tcra-Tcrd* locus with gene segments depicted. Shaded region corresponds to deletion on DJD alleles. **(B)** Average frequencies of V-J_α rearrangements in $CD4^+CD8^+CD3_\varepsilon^{lo}$ thymocytes from WT (left) and DJD (right) mice. Two DJD mice and two WT littermates (mixed 129 and C57BL/6 background) were analyzed in two independent experiments by HTS of 5′ RACE-amplified *Tcra* transcripts. Red bars on left and right edges of heatmaps indicate locations of *Trav15-dv6* family V segments. **(C)** Map depicting difference between average V-J_α rearrangements in DJD and WT mice. Blue represents rearrangements underrepresented in DJD; red represents rearrangements more common in DJD. Black line indicates step-function diagonal with a slope of $4V_\alpha{:}3J_\alpha$ (or 1.33 V_α per J_α, the previously established relationship for the progression of secondary rearrangements across the V and J arrays; Carico et al., 2017). With the origin of the diagonal just distal to *Trav15-2-dv6-2*, the line separates all primary and secondary *Tcra* rearrangements hypothesized to arise as a result of Trav15-dv6 and other central and distal *Tcrd* rearrangements from those expected to occur on alleles that lack such rearrangements. Normalized Shannon's entropy values were 0.953 and 0.950 for replicate WT samples (541,510 and 396,722 unique sequences per sample) and 0.936 and 0.935 for replicate DJD samples (388,593 and 377,173 unique sequences per sample).

thymocytes, a reduction of 74%. We conclude that *Tcrd* rearrangement expands the combinatorial diversity of the *Tcra* repertoire by diversifying V_α use.

Primary *Tcra* rearrangements are poorly represented in the steady-state *Tcra* repertoire. To more robustly investigate the impact of *Tcrd* rearrangement on primary *Tcra* rearrangement, we directly visualized *Tcra* rearrangements in the earliest DP thymocytes. We previously analyzed these cells in mice carrying a tamoxifen-inducible $Tcrd^{CreER}$ allele together with a $Rosa26^{fl\text{-}STOP\text{-}fl\text{-}ZsGreen}$ (hereafter $Rosa26^{ZsG}$) reporter allele (Carico et al., 2017). In these mice, tamoxifen injection causes ZsGreen expression in cells with transcriptionally active *Trdc*, including DN thymocytes, most of which, failing to diverge to the γδT cell fate, progress to rearrange *Tcra* at the DP stage (Madisen et al., 2010; Zhang et al., 2015). To analyze rearrangement on the DJD allele, we mutated *Trac* on the $Tcrd^{CreER}$ allele to prevent annealing of *Trac* 5′ RACE primers (Fig. S1 A). In mice containing $Rosa26^{ZsG}$ and a *Trac*-mutated $Tcrd^{CreER}$ ($Tcrd^{CreER}$ $Trac^{M}$) allele, in combination with either a WT or DJD allele, we analyzed *Tcra* recombination in $ZsGreen^+$ DP thymocytes at 12 h after tamoxifen injection. These primary and early secondary recombinations, in cells that compose <20% of the DP population (Carico et al., 2017), are typically overshadowed by secondary recombinations in the steady-state repertoire. As previously reported (Carico et al., 2017), on WT alleles, we found these recombinations to be restricted to the first half of the J_α array (Fig. 2 A, left panel), with the majority of rearrangements focused on the most proximal J_α segments, *Traj58-Traj48*. V_α use involved the first half of the V_α array, along with a cluster of relatively distal V_α segments. Save for an unexpected reduction in use of *Traj58*, DJD alleles displayed minimal change in overall J_α use (Fig. 2 A, right panel; and Fig. 2 B). However, V_α use on DJD alleles was restricted compared with WT thymocytes, with overall use of segments distal to *Trav15-2-dv6-2*, the most proximal Trav15-dv6 segment, reduced from 59.4% to 32.2% on DJD alleles ($P < 0.0001$ by χ^2 test with Yates's correction). We conclude that *Tcrd* recombination diversifies primary V_α use, leading to a more robust repertoire of secondary rearrangements and ultimately imparting combinatorial diversity upon the *Tcra* repertoire.

Trav15d-1-dv6d-1 and *Trav15-1-dv6-1* rearrangements facilitate distal and central V_α use, respectively, in primary *Tcra* recombinations

Trav15-dv6 segments comprise the most frequent of the distal and central V_δ contributions to the *Tcrd* repertoire; the only other similarly located V_δ gene segments, *Trav14d-3-dv8* and *Trav16d-dv11* (Fig. S2), are rarely used (Chen et al., 2015; Zhao et al., 2016). We observed that in primary recombinations of the WT *Tcra* locus, most central and distal V_α use occurs immediately upstream of Trav15-dv6 family members, particularly *Trav15-1-dv6-1* and *Trav15d-1-dv6d-1* (left panels of Figs. 1 B and 2 A). These early central and distal recombinations are dramatically reduced in DJD mice (Fig. 1 B, right; Fig. 1 C; Fig. 2 A, right; and Fig. 2 B), suggesting that Trav15-dv6 recombinations in DN cells may contribute to diversifying the *Tcra* repertoire. To analyze the impact of Trav15-dv6 rearrangements on *Tcra* recombination, we analyzed two lines of mice, one with a deletion of ∼2 kb spanning *Trav15d-1-dv6d-1* and a second with a similar deletion of *Trav15-1-dv6-1* (Fig. S1 A) for their *Tcra* clonal repertoires. We hypothesized that the loss of either would result in a substantial reduction in recombination events emanating in a diagonal pattern from the most proximal upstream V_α and moving distally through the remaining V_α segments.

Primary and secondary *Tcra* recombinations in the minor diagonal, predicted to occur as a consequence of *Tcrd* rearrangements involving *Trav15d-1-dv6d-1*, represented 3.1% of the *Tcra* repertoire in WT DP thymocytes but only 0.8% of the repertoire in cells lacking *Trav15d-1-dv6d-1* (Fig. 3, A and B, region 1; $P < 0.0001$ by χ^2 test with Yates's correction). Similarly, major diagonal primary and secondary *Tcra* recombinations, predicted to occur as a consequence of *Tcrd* rearrangements involving *Trav15-1-dv6-1*, accounted for 21.2% of the repertoire in WT thymocytes but only 16.6% of the repertoire in cells lacking *Trav15-1-dv6-1* (Fig. 4, A and B, region 2; $P < 0.0001$ by χ^2 test with Yates's correction). In contrast, the representation of minor diagonal *Tcra* recombinations predicted to occur as a consequence of rearrangements involving more distal Trav15-dv6 family members increased slightly in *Trav15-1-dv6-1*–deleted DP cells (Fig. 4, A and B, region 1). In both lines of mice, rearrangements involving V_α segments downstream of the deleted Trav15-dv6 family member increased proportionally (Fig. 3 B, region 3; and Fig. 4 B, region 4). Because reduced minor diagonal *Tcra* rearrangements were observed in both DJD mice and *Trav15d-1-dv6d-1*–deleted mice and reduced major diagonal *Tcra* rearrangements were observed in both DJD mice and *Trav15-1-dv6-1*–deleted mice, we conclude that central and distal *Tcrd* rearrangements involving Trav15-dv6 family members diversify the *Tcra* repertoire.

In thymocytes lacking either *Trav15d-1-dv6d-1* or *Trav15-1-dv6-1*, we observed changes in the *Tcra* repertoire that were not predicted to arise due to loss of *Tcrd* recombination to either segment. In the absence of *Trav15d-1-dv6d-1*, rearrangements between distal V_α and distal J_α segments outside the minor diagonal were reduced to 13.1% of the repertoire from 19.1% in WT; these secondary rearrangements lie on the major diagonal and are predicted to arise from primary rearrangements involving central V_α segments (Fig. 3, A and B, region 2; $P < 0.0001$ by χ^2 test with Yates's correction). Similarly, in *Trav15-1-dv6-1*–deleted mice, major diagonal secondary rearrangements involving central and distal V_α segments were unexpectedly reduced to 37.4% of the repertoire from 43.1% in WT (Fig. 4, A and B, region 3; $P < 0.0001$ by χ^2 test with Yates's correction); these secondary rearrangements are predicted to arise from primary rearrangements involving proximal V_α segments. Moreover, particularly in *Trav15-1-dv6-1*–deleted mice, reduced secondary rearrangements were associated with increased use of V_α segments immediately J_α-proximal to the deleted region (Fig. 4). None of these changes were observed in the DJD repertoire (Fig. 2). This implies that Trav15-dv6 family members impact *Tcra* repertoire diversification by an additional mechanism that is separate from their roles as *Tcrd* recombination substrates. We propose that the *Trav15-1-dv6-1* and *Trav15d-1-dv6d-1* deletions have these additional effects on *Tcra* repertoire diversity because they impair the propagation of secondary *Tcra* rearrangements to V_α segments beyond the deleted region.

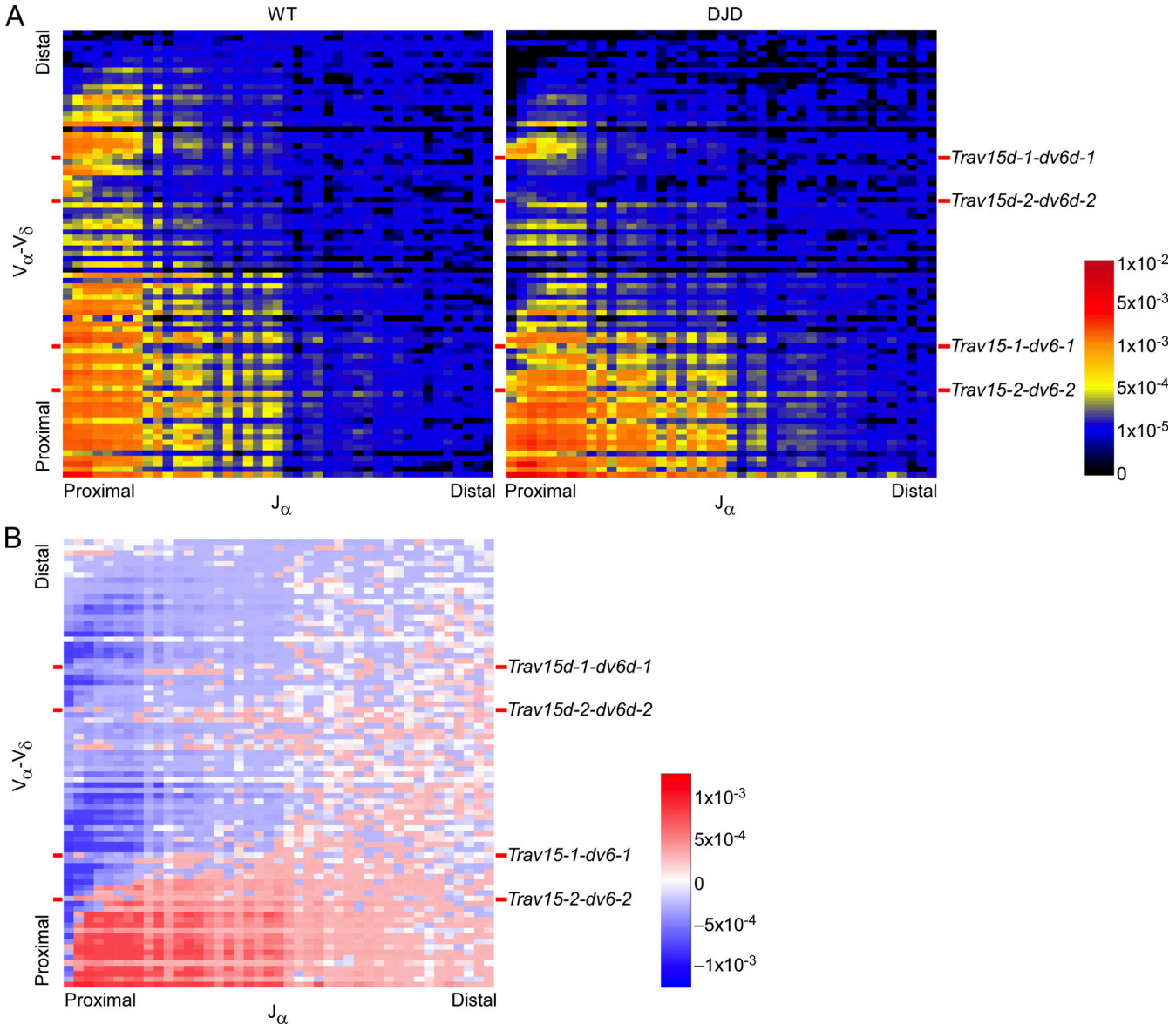

Figure 2. **Early *Tcra* rearrangements are diversified by *Tcrd* recombination. (A)** Average frequencies of V-J_α rearrangements on WT or DJD alleles in $CD4^+CD8^+CD3_\varepsilon^{lo}ZsGreen^+$ thymocytes of mice containing *Rosa26*^{ZsG} and a *Tcrd*^{CreER} *Trac*^{M} allele paired with either a WT or a DJD *Tcra-Tcrd* allele at 12 h after tamoxifen injection. Two DJD and two WT littermates (mixed 129 and C57BL/6 background) were analyzed in two independent experiments. **(B)** Map depicting difference between average V-J_α rearrangements in DJD and WT mice. Normalized Shannon's entropy values were 0.863 and 0.864 for replicate WT samples (81,039 and 116,598 unique sequences per sample) and 0.835 and 0.838 for replicate DJD samples (83,778 and 106,918 unique sequences per sample).

The *Trav15d-1-dv6d-1* and *Trav15-1-dv6-1* deletions encompass regions spanning ∼500 bp upstream of the transcription start site to ∼1 kb downstream of the gene body. These deleted regions are highly conserved between Trav15-1-dv6 family members and include the promoter, the RSS, and downstream E-box sites that are highly accessible and, by chromatin immunoprecipitation followed by sequencing (ChIP-seq), are occupied by E2A at levels surpassed within the *Tcra-Tcrd* locus only by *Tcra* enhancer E-box sites (Fig. S3; Heng et al., 2008; Roy et al., 2018; Yoshida et al., 2019). Loss of the Trav15-dv6 RSS could inhibit more distal secondary rearrangements if the propagation of sequential rearrangements requires closely spaced RSSs. However, Trav15-dv6 family members were not found to be frequently recombined in the WT *Tcra* repertoire, suggesting that Trav15-dv6 RSSs are often skipped during secondary rearrangements (Fig. 1 B). Moreover, the distance between the nearest functional V_α segments flanking Trav15-dv6 is reduced from ∼37 kb to ∼35 kb on the deleted alleles. We considered that *Trav15-dv6* deletion might influence secondary rearrangements by disrupting the CCCTC binding factor (CTCF)–mediated chromatin loop organization. However, binding sites for CTCF were not disrupted on the *Trav15d-1-dv6d-1*– or *Trav15-1-dv6-1*–deleted alleles (Shih et al., 2012), and the deletions do not obviously create de novo CTCF binding sites (Martin et al., 2011).

It remains possible that Trav15-dv6 segments influence secondary *Tcra* recombinations via effects on chromatin accessibility mediated by flanking *cis*-acting elements. The *Trav15-1-dv6-1*

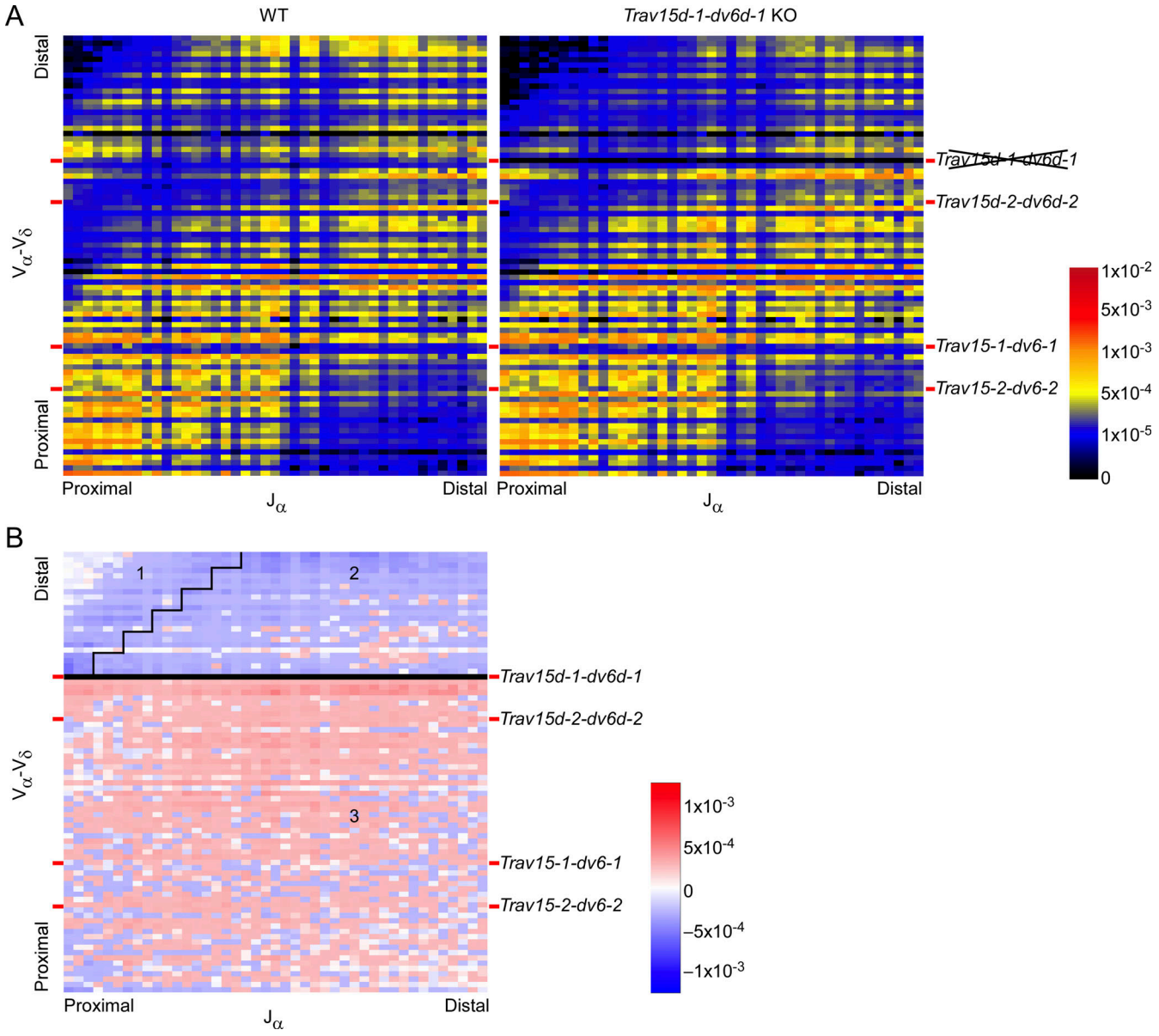

Figure 3. **Reduced distal V_α use in *Trav15d-1-dv6d-1* KO mice. (A)** Average frequencies of V-J_α rearrangements in $CD4^+CD8^+CD3_\varepsilon^{lo}$ thymocytes of mice carrying WT (left) or *Trav15d-1-dv6d-1* KO (right) *Tcra-Tcrd* alleles. Although irrelevant for this analysis, WT and KO *Tcra-Tcrd* alleles also carry $Tcrd^{CreER}$ (see Materials and methods). Two littermates per genotype (C57BL/6 background) were analyzed in two independent experiments. **(B)** Map depicting difference between average V-J_α rearrangements on *Trav15d-1-dv6d-1* KO and WT alleles. Region 1, primary and secondary *Tcra* rearrangements predicted to depend on use of *Trav15d-1-dv6d-1* in *Tcrd* recombination. Region 2, secondary rearrangements upstream of *Trav15d-1-dv6d-1* expected to arise from primary and secondary recombinations downstream of *Trav15d-1-dv6d-1*. Region 3, primary and secondary rearrangements downstream of *Trav15d-1-dv6d-1*. Normalized Shannon's entropy values were 0.944 and 0.947 for replicate WT samples (171,982 and 318,404 unique sequences per sample) and 0.938 and 0.942 for replicate *Trav15d-1-dv6d-1* samples (219,968 and 304,900 unique sequences per sample).

promoter drives accessibility, transcription, and recombination of *Trav15-1-dv6-1* in DN thymocytes (Naik et al., 2015) but displays only modest accessibility and is not expected to influence neighboring V segments (Heng et al., 2008; Yoshida et al., 2019). Perhaps a better candidate is the highly accessible downstream E2A-bound element (Fig. S3). E2A is a known regulator of *Tcrd* recombination and γδT cell fate (Bain et al., 1999) and may influence Trav15-dv6 rearrangement in DN thymocytes. As the E2A-bound region remains highly accessible in DP thymocytes, it could have extended effects on accessibility and RAG binding at RCs that form downstream of Trav15-dv6 family members during secondary rearrangement or on V_α substrates upstream of Trav15-dv6 family members. The *cis* region may alternatively serve as a mediator of locus structure to facilitate recombination; such features have been observed at other AgR loci (Barajas-Mora et al., 2019). Further exploration of this phenomenon is warranted to better understand these perturbations of secondary *Tcra* rearrangements on *Trav15d-1-dv6d-1*– and *Trav15-1-dv6-1*–deleted alleles.

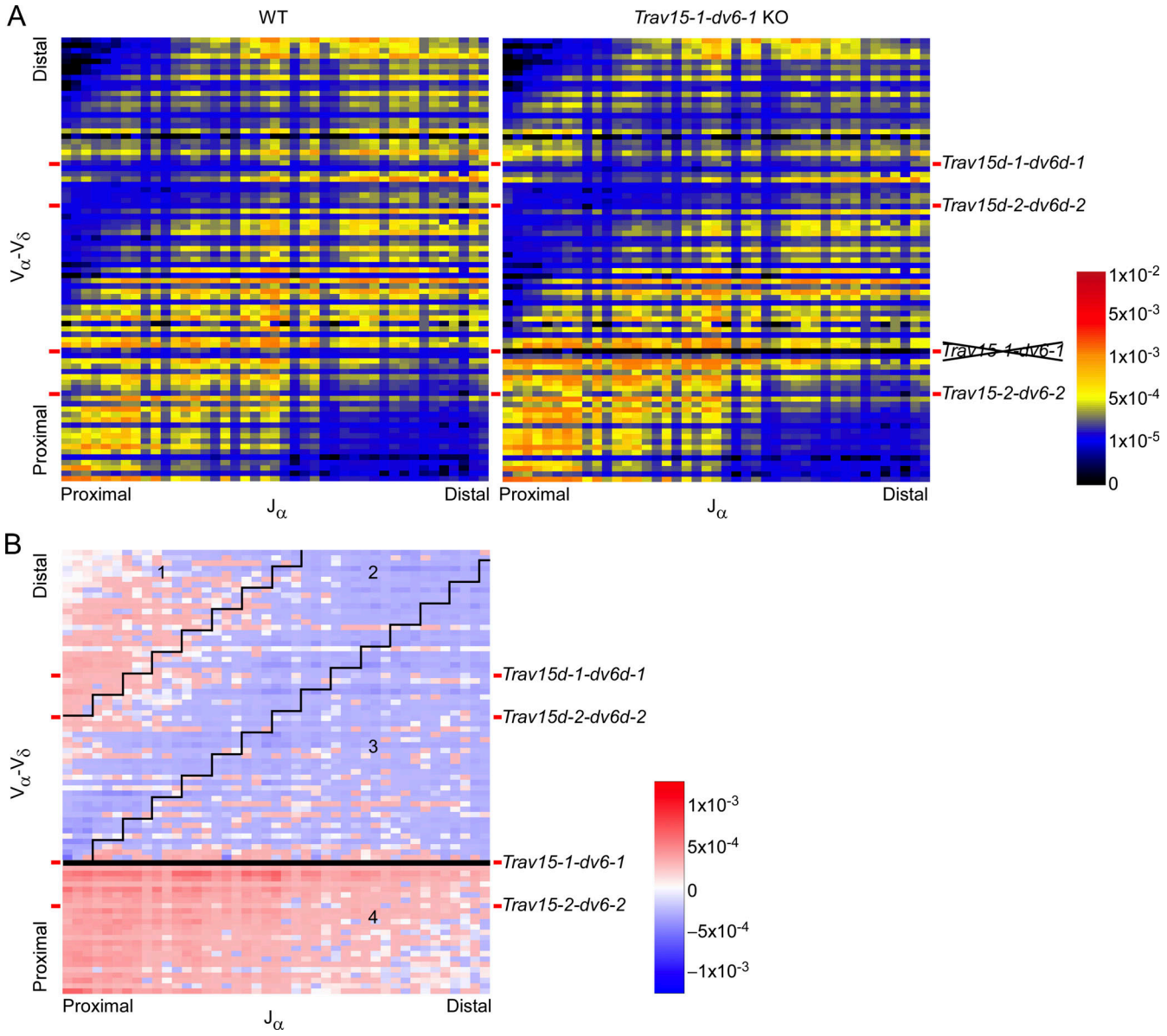

Figure 4. **Reduced central V_α use in *Trav15-1-dv6-1* KO mice. (A)** Average frequencies of V-J_α rearrangements in $CD4^+CD8^+CD3_\varepsilon^{lo}$ thymocytes of mice carrying WT (left) or *Trav15-1-dv6-1* KO (right) *Tcra-Tcrd* alleles. Although irrelevant for this analysis, WT and KO *Tcra-Tcrd* alleles also carry $Tcrd^{CreER}$ (see Materials and methods). Two littermates per genotype (C57BL/6 background) were analyzed in two independent experiments. **(B)** Map depicting difference between average V-J_α rearrangements on *Trav15-1-dv6-1* KO and WT alleles. Region 1, primary and secondary *Tcra* rearrangements predicted to depend on *Trav15d-1-dv6d-1* and *Trav15d-2-dv6d-2 Tcrd* rearrangements. Region 2, primary and secondary *Tcra* rearrangements predicted to depend on *Trav15-1-dv6-1 Tcrd* rearrangements. Region 3, secondary *Tcra* rearrangements upstream of *Trav15-1-dv6-1* expected to arise from primary and secondary *Tcra* recombinations downstream of *Trav15-1-dv6-1*. Region 4, primary and secondary *Tcra* rearrangements downstream of *Trav15-1-dv6-1*. Normalized Shannon's entropy values were 0.950 and 0.947 for replicate WT samples (262,146 and 324,511 unique sequences per sample) and 0.947 and 0.939 for replicate *Trav15-1-dv6-1* samples (223,783 and 264,507 unique sequences per sample).

Our repertoire studies emphasize that capture of V gene segments within the *Tcra-Tcrd* locus occurs via distinct mechanisms during *Tcrd* and *Tcra* rearrangement. Capture of V_δ gene segments by the *Tcrd* RC in DN thymocytes can occur over very long distances. By contrast, capture of V_α gene segments by *Tcra* RCs appears to occur predominantly as a result of short-range interactions once those segments are brought into proximity of the RC by prior rounds of rearrangement. One exception is the residual rearrangement of central and distal V_α segments in early rearrangements on DJD alleles (Fig. 2 A, right panel); the cluster of rearrangements between V segments upstream of *Trav15d-2-dv6d-2* and J segments *Traj58-Traj48* is not ablated, but rather reduced from 11.4% to 3.5% ($P < 0.0001$ by χ^2 test with Yates's correction). We think that these rearrangements, which include *Trav15d-1-dv6d-1*, may result from residual chromatin marks carried over from DN thymocytes in the absence of *Tcrd* recombination, facilitating DN-like V capture in early DP thymocytes.

The change in the mode of V segment capture between the DN and DP stages of thymocyte development correlates with a conformational change in the *Tcra-Tcrd* locus, with the V array being contracted in DN and extended in DP (Shih and Krangel, 2010). Prior work has shown that long-range capture of V_H segments by the *Igh* RC in pro-B cells occurs via long-range RAG scanning and cohesin-mediated loop extrusion, facilitated by reduced expression of the cohesin unloader *Wapl* (Hu et al., 2015; Lin et al., 2018; Ba et al., 2020; Hill et al., 2020; Dai et al., 2021). However, RAG scanning from the *Tcrd* RC appears to be effectively contained within an 80-kb chromatin loop domain formed by the INT1-2 and T early α CTCF binding elements in DN thymocytes (Chen et al., 2015; Zhao et al., 2016). This suggests that long-range capture of V_δ gene segments may occur via diffusion. In contrast, short-range V_α capture by the *Tcra* RC in DP thymocytes can be envisioned to occur either by relatively short-range RAG scanning or by diffusive interactions. Regardless, our data suggest that *Tcra* repertoire diversity in mice results from synergy between two different modes of V segment capture. We expect that our conclusions on *Tcra* repertoire diversity in mice likely extend to humans, since the human *Tcra-Tcrd* locus is similarly organized with V_δ gene segments distributed among central and distal V_α gene segments.

Materials and methods

Mice

To generate DJD mice, female C57BL/6J mice were mated to male strain 129 mice. The resulting F1 embryos were subjected to pronuclear injection of reagents for two guide–mediated CRISPR/Cas9 (Cong et al., 2013; Singh et al., 2015) to delete an ∼24.3-kb region spanning *Trdd1-Trdj2* at the *Tcra-Tcrd* locus. The upstream guide sequence was 5′-GACTCACCTGTTATCAAACT-3′, and the downstream guide sequence was 5′-ATAATGCTAAAA TTACCTGC-3′. Offspring were screened for deletion on the 129 *Tcra-Tcrd* allele using PCR and Sanger sequencing (Duke University DNA Analysis Facility). Appropriately targeted mice of mixed C57BL/6J and 129 genetic background were crossed once to strain 129, and DJD heterozygotes were then intercrossed to obtain homozygous WT and DJD littermates for analysis.

Tcrd$^{CreER/CreER}$ *Rosa26*$^{ZsG/ZsG}$ mice, with modified strain 129 *Tcra-Tcrd* alleles on a C57BL/6 genetic background (backcrossed >10 generations), were described previously (Zhang et al., 2015). These mice were further modified by deletion of 138 bp spanning the 5′ portion of *Trac* exon 1 to generate *Tcrd*$^{CreER/CreER}$ *Trac*$^{M/+}$ *Rosa26*$^{ZsG/ZsG}$ mice. Two guide–mediated CRISPR/Cas9 targeting was accomplished by electroporation using upstream guide 5′-CAGGCAAGAGCGGAACTCTC-3′ and downstream guide 5′-GAGACCGAGGATCTTTTAAC-3′. The founder mouse was backcrossed once to *Tcrd*$^{CreER/CreER}$ *Rosa26*$^{ZsG/ZsG}$, and mice heterozygous for the *Trac* mutation were then intercrossed to obtain *Tcrd*$^{CreER/CreER}$ *Trac*$^{M/M}$ *Rosa26*$^{ZsG/ZsG}$ mice. These were then crossed to DJD heterozygotes to obtain littermates containing a *Rosa26*^{ZsG} allele and *Tcrd*^{CreER} *Trac*^{M} allele paired with either a WT 129 or DJD 129 *Tcra-Tcrd* allele on a mixed C57BL/6 and 129 genetic background.

Trav15-1-dv6-1 and *Trav15d-1-dv6d-1* deletions were generated in *Tcrd*$^{CreER/CreER}$ *Rosa26*$^{ZsG/ZsG}$ *Id3*$^{f/f}$ mice (Madisen et al., 2010; Guo et al., 2011; Zhang et al., 2015) containing modified strain 129 *Tcra-Tcrd* alleles on a C57BL/6 genetic background (backcrossed >10 generations). Two-guide mediated CRISPR/Cas9 targeting was accomplished by electroporation using upstream guide 5′-TCTTCCCTTAAAGAGTGATA-3′, and downstream guide 5′-GACATTAGAGTCCCTTAAAG-3′. Offspring were screened by PCR and Sanger sequencing. Deletions of *Trav15-1-dv6-1* and *Trav15d-1-dv6d-1* were detected in different founders and maintained separately. Appropriately targeted mice were crossed to *Tcrd*$^{CreER/CreER}$ *Rosa26*$^{ZsG/ZsG}$ *Id3*$^{f/f}$ mice to obtain *Rosa26*$^{ZsG/ZsG}$ *Id3*$^{f/f}$ mice containing a *Trav15-1-dv6-1* KO *Tcrd*^{CreER} or a *Trav15d-1-dv6d-1* KO *Tcrd*^{CreER} allele paired with a *Tcrd*^{CreER} allele on a C57BL/6 genetic background. Intercrossing of *Trav15-1-dv6-1* KO heterozygous mice generated littermates containing either homozygous *Trav15-1-dv6-1* KO *Tcrd*^{CreER} or *Tcrd*^{CreER} alleles for analysis. Intercrossing of *Trav15d-1-dv6d-1* KO heterozygous mice generated littermates containing either homozygous *Trav15d-1-dv6d-1* KO *Tcrd*^{CreER} or *Tcrd*^{CreER} alleles for analysis.

All CRISPR/Cas9-mediated deletions were performed by the Duke University Transgenic and Knockout Mouse Shared Resource. Mice were sacrificed at 4–5 wk of age. Both male and female mice were used; no differences were observed on the basis of sex. All mice were handled under protocols approved by the Duke University Institutional Animal Care and Use Committee and maintained in specific pathogen–free conditions.

Cell collection and flow cytometry

For analysis of thymocyte subpopulations, thymi were collected from mice at 3–4 wk of age. To sort DP thymocytes for repertoire analysis, thymi were collected from mice at 4–5 wk of age. To label developing thymocytes with ZsGreen, mice were injected i.p. with a single 100-µl dose of 10 mg/ml tamoxifen (Sigma-Aldrich) in corn oil (Sigma-Aldrich) 12 h before sacrifice.

To obtain preselection DP thymocytes (defined as CD4$^+$CD8$^+$Lin$^-$7AAD$^-$CD3ε^{lo}), total thymocytes were stained with anti-CD4 (GK1.5), anti-CD8α (53-6.7), anti-CD3$_\varepsilon$ (145-2C11), 7AAD, and PE-Cy5–conjugated lineage (Lin) markers anti-B220 (RA3-6B2), anti-CD11b (M1/70), anti-CD11c (N418), anti-F4/80 (BM8), anti–Gr-1 (RB6-8C5; Invitrogen), and anti–Ter-119 (TER-119). Preselection DP thymocytes from tamoxifen-injected mice were additionally sorted for ZsGreen$^+$. For analysis of thymocyte subpopulations, total thymocytes were additionally stained with Pacific Blue anti-CD25 (PC61), allophycocyanin-Cy7 anti-cKit (2B8), and allophycocyanin anti-γδTCR (GL3). All antibodies were purchased from BioLegend, unless otherwise specified.

Tcra repertoire library preparation

Tcra sequencing libraries were prepared as previously described (Carico et al., 2017). Briefly, RNA was extracted using TRIzol (Life Technologies) from sorted preselection DP thymocytes. 5′ RACE was performed on total RNA as previously described (Pinto and Lindblad, 2010; Quigley et al., 2011; Carico et al., 2017), with minor modifications. 700 ng RNA was used as input for template-switch 5′ RACE and cDNA synthesis using

SuperScript II (Thermo Fisher Scientific). Kapa HiFi polymerase in 1× Kapa HiFi buffer (Kapa Biosystems) was used for all PCRs in 50 µl total volume per reaction; eight reactions were performed per sample for each round of PCR. PCR products were pooled and purified using the QIAquick PCR purification kit (Qiagen) per the manufacturer's specifications. Purified products of the first PCR were subjected to a second round of PCR amplification as described (Kozich et al., 2013; Carico et al., 2017) to ligate barcodes and Illumina adapter sequences. Libraries were then pooled and purified using the QIAquick PCR purification kit and resuspended in nuclease-free water.

Tcra repertoire sequencing and analysis

Sequencing and analysis were performed as previously described (Carico et al., 2017), with minor modifications. Briefly, barcoded libraries were pooled and sequenced by the Duke University Sequencing and Genomic Technologies Shared Resource using 300-nt paired-end reads on the Illumina MiSeq platform (version 3 chemistry). Agilent Bioanalyzer analysis was used to determine library molarity and quality, and size selection was performed by the Duke University Sequencing and Genomic Technologies Shared Resource for further purification. A PhiX control library and custom primers were added to the standard Illumina primer mix, as previously described (Carico et al., 2017). Libraries were demultiplexed and assessed for quality and yield using Illumina MiSeq Reporter software.

Analysis was performed using MiXCR (version 3.0.7; Bolotin et al., 2015). The reference library was edited to permit alignments only to 129 sequences (Bosc and Lefranc, 2003). The "align" command was used to align sequencing reads to this reference library. The "assemble" command was then used to identify clones with sequences spanning CDR2 through CDR3. Each clone was assigned to the corresponding V and J segments. The "exportClones" command produced a human-readable form of these data; alignment was manually reviewed. Sequences aligning to pseudogenes and other very infrequently uses genes were manually removed, including *Traj61*, *Traj41*, *Traj25*, *Trav5d-2*, *Trav7d-6*, *Trav7-6*, and *Trav18*. *Trav11* and *Trav11d* are not distinguishable; both were maintained in this analysis, but the computed distribution of reads between the segments should be ignored. The VDJtools (Shugay et al., 2015) command PlotFancyVJUsage was used to calculate clonal frequencies of V-J recombinations. In R (version 3.3.3; R Core Team, 2020), and heatmaps were generated using the gplots (Warnes et al., 2009) and RColorBrewer (Neuwirth, 2014) packages. For difference maps, the WT repertoire was subtracted from the mutant repertoire. Repertoire differences were reported for regions demarcated by step-function diagonals with a slope of $4V_\alpha{:}3J_\alpha$ (or 1.33 V_α per J_α), the previously established relationship for the progression of secondary rearrangements across the V and J arrays (Carico et al., 2017). Total numbers of unique sequences in each region were combined from two replicates per genotype, and differences between genotypes were evaluated by two-tailed χ^2 test with Yates's correction for continuity, using GraphPad Prism 6 software. When determining the regional changes to the repertoire in *Trav15d-1-dv6d-1*– and *Trav15-1-dv6-1*–deleted models, the deleted segment in each case was excluded from analysis.

Tcra repertoire sequencing data are deposited in the Gene Expression Omnibus under accession no. GSE186044.

Global Shannon's entropy calculation

Global V-J pair diversity was measured by Shannon entropy index (H). Shannon entropy quantifies both abundance and degree of unevenness of all distinct V-J pairs in a sample. A higher H value indicates more even distribution for distinct V-J pairs, while a lower value suggests that a dominant V-J type occupies overall pairs. The Shannon diversity (H) was calculated using the following equation:

$$H = -\sum_{i=1}^{S} p_i \log p_i,$$

where p_i is the fraction of i-th V-J pairs in a sample, and S is the total combinations of V-J pairs. In this study, S = 3,569 (83 V × 43 J). We then normalized H to the maximum H_{max} using the following equation:

$$E_H = \frac{H}{H_{max}}.$$

The normalized Shannon index E_H is bounded from 0 to 1, and a value of 1 means all V-J pairs have the same frequency.

E2A ChIP-seq analysis

E2A ChIP-seq from sorted DP thymocytes ($CD1dTet^-CD4^+CD8^+$) isolated from $Id2^{f/f}$ $Id3^{f/f}$ *Lck*-Cre C57BL/6 mice was previously reported (Roy et al., 2018). Here, alignment was performed to mm10 using Bowtie2 (version 2.3.4.1), allowing multiple read alignment (k = 3) to account for sequence similarity within the *Tcra-Tcrd* locus; all other parameters were set to default. Peak calling was performed using MACS2 (version 2.1.1.20160309); default options were used. Data visualization was performed using the Integrative Genomics Viewer (version 2.8.2).

Online supplemental material

Fig. S1 shows characterization of mouse strain mutations and thymocyte cell populations in DJD mice. Fig. S2 shows the WT strain 129 *Tcra* combinatorial repertoire with gene segments and secondary *Tcra* recombination diagonals identified. Fig. S3 shows *Tcra-Tcrd* locus E2A ChIP tracks.

Acknowledgments

We thank Lunden Simpson and Abani Naik for comments on the manuscript and Qi-Jing Li for helpful discussions.

This research was supported in part by National Institutes of Health grants R01 GM41052 and R35 GM136284 (to M.S. Krangel) and P01 AI102853 (to Y. Zhuang).

Author contributions: D.J. Dauphars, A. Mihai, Y. Zhuang, and M.S. Krangel designed the study; D.J. Dauphars and A. Mihai performed the experiments; D.J. Dauphars, A. Mihai, and L. Wang analyzed the data; and D.J. Dauphars, A. Mihai, L. Wang, and M.S. Krangel wrote the manuscript.

Disclosures: The authors declare no competing interests exist.

Submitted: 23 July 2021
Revised: 4 November 2021
Accepted: 2 December 2021

References

Ba, Z., J. Lou, A.Y. Ye, H.-Q. Dai, E.W. Dring, S.G. Lin, S. Jain, N. Kyritsis, K.-R. Kieffer-Kwon, R. Casellas, and F.W. Alt. 2020. CTCF orchestrates long-range cohesin-driven V(D)J recombinational scanning. *Nature.* 586: 305–310. https://doi.org/10.1038/s41586-020-2578-0

Bain, G., W.J. Romanow, K. Albers, W.L. Havran, and C. Murre. 1999. Positive and negative regulation of V(D)J recombination by the E2A proteins. *J. Exp. Med.* 189:289–300. https://doi.org/10.1084/jem.189.2.289

Barajas-Mora, E.M., E. Kleiman, J. Xu, N.C. Carrico, H. Lu, E.M. Oltz, C. Murre, and A.J. Feeney. 2019. A B-cell-specific enhancer orchestrates nuclear architecture to generate a diverse antigen receptor repertoire. *Mol. Cell.* 73:48–60.e5. https://doi.org/10.1016/j.molcel.2018.10.013

Bolotin, D.A., S. Poslavsky, I. Mitrophanov, M. Shugay, I.Z. Mamedov, E.V. Putintseva, and D.M. Chudakov. 2015. MiXCR: software for comprehensive adaptive immunity profiling. *Nat. Methods.* 12:380–381. https://doi.org/10.1038/nmeth.3364

Bosc, N., and M.P. Lefranc. 2003. The mouse (*Mus musculus*) T cell receptor alpha (TRA) and delta (TRD) variable genes. *Dev. Comp. Immunol.* 27: 465–497. https://doi.org/10.1016/S0145-305X(03)00027-2

Buch, T., F. Rieux-Laucat, I. Förster, and K. Rajewsky. 2002. Failure of HY-specific thymocytes to escape negative selection by receptor editing. *Immunity.* 16:707–718. https://doi.org/10.1016/S1074-7613(02)00312-6

Capone, M., R.D. Hockett Jr., and A. Zlotnik. 1998. Kinetics of T cell receptor β, γ, and δ rearrangements during adult thymic development: T cell receptor rearrangements are present in CD44(+)CD25(+) Pro-T thymocytes. *Proc. Natl. Acad. Sci. USA.* 95:12522–12527. https://doi.org/10.1073/pnas.95.21.12522

Carico, Z., and M.S. Krangel. 2015. Chromatin dynamics and the development of the TCRα and TCRδ repertoires. *Adv. Immunol.* 128:307–361. https://doi.org/10.1016/bs.ai.2015.07.005

Carico, Z.M., K. Roy Choudhury, B. Zhang, Y. Zhuang, and M.S. Krangel. 2017. *Tcrd* rearrangement redirects a processive *Tcra* recombination program to expand the *Tcra* repertoire. *Cell Rep.* 19:2157–2173. https://doi.org/10.1016/j.celrep.2017.05.045

Chen, L., Z. Carico, H.-Y. Shih, and M.S. Krangel. 2015. A discrete chromatin loop in the mouse Tcra-Tcrd locus shapes the TCRδ and TCRα repertoires. *Nat. Immunol.* 16:1085–1093. https://doi.org/10.1038/ni.3232

Cong, L., F.A. Ran, D. Cox, S. Lin, R. Barretto, N. Habib, P.D. Hsu, X. Wu, W. Jiang, L.A. Marraffini, and F. Zhang. 2013. Multiplex genome engineering using CRISPR/Cas systems. *Science.* 339:819–823. https://doi.org/10.1126/science.1231143

Dai, H.-Q., H. Hu, J. Lou, A.Y. Ye, Z. Ba, X. Zhang, Y. Zhang, L. Zhao, H.S. Yoon, A.M. Chapdelaine-Williams, et al. 2021. Loop extrusion mediates physiological Igh locus contraction for RAG scanning. *Nature.* 590: 338–343. https://doi.org/10.1038/s41586-020-03121-7

Glusman, G., L. Rowen, I. Lee, C. Boysen, J.C. Roach, A.F.A. Smit, K. Wang, B.F. Koop, and L. Hood. 2001. Comparative genomics of the human and mouse T cell receptor loci. *Immunity.* 15:337–349. https://doi.org/10.1016/S1074-7613(01)00200-X

Guo, Z., H. Li, M. Han, T. Xu, X. Wu, and Y. Zhuang. 2011. Modeling Sjögren's syndrome with Id3 conditional knockout mice. *Immunol. Lett.* 135:34–42. https://doi.org/10.1016/j.imlet.2010.09.009

Hawwari, A., and M.S. Krangel. 2007. Role for rearranged variable gene segments in directing secondary T cell receptor α recombination. *Proc. Natl. Acad. Sci. USA.* 104:903–907. https://doi.org/10.1073/pnas.0608248104

Helmink, B.A., and B.P. Sleckman. 2012. The response to and repair of RAG-mediated DNA double-strand breaks. *Annu. Rev. Immunol.* 30:175–202. https://doi.org/10.1146/annurev-immunol-030409-101320

Heng, T.S.P., M.W. Painter, K. Elpek, V. Lukacs-Kornek, N. Mauermann, S.J. Turley, D. Koller, F.S. Kim, A.J. Wagers, N. Asinovski, et al. Immunological Genome Project Consortium. 2008. The Immunological Genome Project: networks of gene expression in immune cells. *Nat. Immunol.* 9: 1091–1094. https://doi.org/10.1038/ni1008-1091

Hill, L., A. Ebert, M. Jaritz, G. Wutz, K. Nagasaka, H. Tagoh, D. Kostanova-Poliakova, K. Schindler, Q. Sun, P. Bönelt, et al. 2020. Wapl repression by Pax5 promotes V gene recombination by Igh loop extrusion. *Nature.* 584:142–147. https://doi.org/10.1038/s41586-020-2454-y

Hu, J., Y. Zhang, L. Zhao, R.L. Frock, Z. Du, R.M. Meyers, F.L. Meng, D.G. Schatz, and F.W. Alt. 2015. Chromosomal loop domains direct the recombination of antigen receptor genes. *Cell.* 163:947–959. https://doi.org/10.1016/j.cell.2015.10.016

Itohara, S., P. Mombaerts, J. Lafaille, J. Iacomini, A. Nelson, A.R. Clarke, M.L. Hooper, A. Farr, and S. Tonegawa. 1993. T cell receptor δ gene mutant mice: independent generation of α β T cells and programmed rearrangements of γ δ TCR genes. *Cell.* 72:337–348. https://doi.org/10.1016/0092-8674(93)90112-4

Jhunjhunwala, S., M.C. van Zelm, M.M. Peak, and C. Murre. 2009. Chromatin architecture and the generation of antigen receptor diversity. *Cell.* 138: 435–448. https://doi.org/10.1016/j.cell.2009.07.016

Ji, Y., W. Resch, E. Corbett, A. Yamane, R. Casellas, and D.G. Schatz. 2010. The in vivo pattern of binding of RAG1 and RAG2 to antigen receptor loci. *Cell.* 141:419–431. https://doi.org/10.1016/j.cell.2010.03.010

Kozich, J.J., S.L. Westcott, N.T. Baxter, S.K. Highlander, and P.D. Schloss. 2013. Development of a dual-index sequencing strategy and curation pipeline for analyzing amplicon sequence data on the MiSeq Illumina sequencing platform. *Appl. Environ. Microbiol.* 79:5112–5120. https://doi.org/10.1128/AEM.01043-13

Lin, S.G., Z. Ba, F.W. Alt, and Y. Zhang. 2018. RAG chromatin scanning during V(D)J recombination and chromatin loop extrusion are related processes. *Adv. Immunol.* 139:93–135. https://doi.org/10.1016/bs.ai.2018.07.001

Livak, F., H.T. Petrie, I.N. Crispe, and D.G. Schatz. 1995. In-frame TCR δ gene rearrangements play a critical role in the α β/γ δ T cell lineage decision. *Immunity.* 2:617–627. https://doi.org/10.1016/1074-7613(95)90006-3

Madisen, L., T.A. Zwingman, S.M. Sunkin, S.W. Oh, H.A. Zariwala, H. Gu, L.L. Ng, R.D. Palmiter, M.J. Hawrylycz, A.R. Jones, et al. 2010. A robust and high-throughput Cre reporting and characterization system for the whole mouse brain. *Nat. Neurosci.* 13:133–140. https://doi.org/10.1038/nn.2467

Martin, D., C. Pantoja, A. Fernández Miñán, C. Valdes-Quezada, E. Moltó, F. Matesanz, O. Bogdanović, E. de la Calle-Mustienes, O. Domínguez, L. Taher, et al. 2011. Genome-wide CTCF distribution in vertebrates defines equivalent sites that aid the identification of disease-associated genes. *Nat. Struct. Mol. Biol.* 18:708–714. https://doi.org/10.1038/nsmb.2059

Monroe, R.J., B.P. Sleckman, B.C. Monroe, B. Khor, S. Claypool, R. Ferrini, L. Davidson, and F.W. Alt. 1999. Developmental regulation of TCR delta locus accessibility and expression by the TCR delta enhancer. *Immunity.* 10:503–513. https://doi.org/10.1016/S1074-7613(00)80050-3

Naik, A.K., A. Hawwari, and M.S. Krangel. 2015. Specification of Vδ and Vα usage by Tcra/Tcrd locus V gene segment promoters. *J. Immunol.* 194: 790–794. https://doi.org/10.4049/jimmunol.1402423

Nakajima, P.B., J.P. Menetski, D.B. Roth, M. Gellert, and M.J. Bosma. 1995. V-D-J rearrangements at the T cell receptor δ locus in mouse thymocytes of the α β lineage. *Immunity.* 3:609–621. https://doi.org/10.1016/1074-7613(95)90132-9

Neuwirth, E. 2014. RColorBrewer: ColorBrewer Palettes. https://CRAN.R-project.org/package=RColorBrewer (accessed March 14, 2021).

Petrie, H.T., F. Livak, D.G. Schatz, A. Strasser, I.N. Crispe, and K. Shortman. 1993. Multiple rearrangements in T cell receptor α chain genes maximize the production of useful thymocytes. *J. Exp. Med.* 178:615–622. https://doi.org/10.1084/jem.178.2.615

Petrie, H.T., F. Livak, D. Burtrum, and S. Mazel. 1995. T cell receptor gene recombination patterns and mechanisms: cell death, rescue, and T cell production. *J. Exp. Med.* 182:121–127. https://doi.org/10.1084/jem.182.1.121

Pinto, F.L., and P. Lindblad. 2010. A guide for in-house design of template-switch-based 5′ rapid amplification of cDNA ends systems. *Anal. Biochem.* 397:227–232. https://doi.org/10.1016/j.ab.2009.10.022

Quigley, M.F., J.R. Almeida, D.A. Price, and D.C. Douek. 2011. Unbiased molecular analysis of T cell receptor expression using template-switch anchored RT-PCR. *Curr. Protoc. Immunol.* 94:10.33.1–10.33.16. https://doi.org/10.1002/0471142735.im1033s94

R Core Team. 2020. R: A language and environment for statistical computing. R Foundation for Statistical Computing. https://www.R-project.org/.

Roy, S., A.J. Moore, C. Love, A. Reddy, D. Rajagopalan, S.S. Dave, L. Li, C. Murre, and Y. Zhuang. 2018. Id proteins suppress E2A-driven invariant natural killer T cell development prior to TCR selection. *Front. Immunol.* 9:42. https://doi.org/10.3389/fimmu.2018.00042

Schatz, D.G., and Y. Ji. 2011. Recombination centres and the orchestration of V(D)J recombination. *Nat. Rev. Immunol.* 11:251–263. https://doi.org/10.1038/nri2941

Shih, H.-Y., and M.S. Krangel. 2010. Distinct contracted conformations of the Tcra/Tcrd locus during Tcra and Tcrd recombination. *J. Exp. Med.* 207: 1835–1841. https://doi.org/10.1084/jem.20100772

Shih, H.-Y., J. Verma-Gaur, A. Torkamani, A.J. Feeney, N. Galjart, and M.S. Krangel. 2012. Tcra gene recombination is supported by a Tcra enhancer- and CTCF-dependent chromatin hub. *Proc. Natl. Acad. Sci. USA.* 109:E3493–E3502. https://doi.org/10.1073/pnas.1214131109

Shugay, M., D.V. Bagaev, M.A. Turchaninova, D.A. Bolotin, O.V. Britanova, E.V. Putintseva, M.V. Pogorelyy, V.I. Nazarov, I.V. Zvyagin, V.I. Kirgizova, et al. 2015. VDJtools: unifying post-analysis of T cell receptor repertoires. *PLOS Comput. Biol.* 11:e1004503. https://doi.org/10.1371/journal.pcbi.1004503

Singh, P., J.C. Schimenti, and E. Bolcun-Filas. 2015. A mouse geneticist's practical guide to CRISPR applications. *Genetics.* 199:1–15. https://doi.org/10.1534/genetics.114.169771

Sleckman, B.P., B. Khor, R. Monroe, and F.W. Alt. 1998. Assembly of productive T cell receptor δ variable region genes exhibits allelic inclusion. *J. Exp. Med.* 188:1465–1471. https://doi.org/10.1084/jem.188.8.1465

Thompson, S.D., J. Pelkonen, and J.L. Hurwitz. 1990. First T cell receptor alpha gene rearrangements during T cell ontogeny skew to the 5′ region of the J alpha locus. *J. Immunol.* 145:2347–2352.

Wang, F., C.Y. Huang, and O. Kanagawa. 1998. Rapid deletion of rearranged T cell antigen receptor (TCR) Valpha-Jalpha segment by secondary rearrangement in the thymus: role of continuous rearrangement of TCR α chain gene and positive selection in the T cell repertoire formation. *Proc. Natl. Acad. Sci. USA.* 95:11834–11839. https://doi.org/10.1073/pnas.95.20.11834

Warnes, G.R., B. Bolker, L. Bonebakker, R. Gentleman, W. Huber, A. Liaw, T. Lumley, M. Maechler, A. Magnusson, S. Moeller, et al. 2009. gplots: Various R programming tools for plotting data. https://CRAN.R-project.org/package=gplots (accessed March 14, 2021).

Yoshida, H., C.A. Lareau, R.N. Ramirez, S.A. Rose, B. Maier, A. Wroblewska, F. Desland, A. Chudnovskiy, A. Mortha, C. Dominguez, et al. Immunological Genome Project. 2019. The cis-Regulatory Atlas of the Mouse Immune System. *Cell.* 176:897–912.e20. https://doi.org/10.1016/j.cell.2018.12.036

Zhang, B., J. Wu, Y. Jiao, C. Bock, M. Dai, B. Chen, N. Chao, W. Zhang, and Y. Zhuang. 2015. Differential requirements of TCR signaling in homeostatic maintenance and function of dendritic epidermal T cells. *J. Immunol.* 195:4282–4291. https://doi.org/10.4049/jimmunol.1501220

Zhao, L., R.L. Frock, Z. Du, J. Hu, L. Chen, M.S. Krangel, and F.W. Alt. 2016. Orientation-specific RAG activity in chromosomal loop domains contributes to Tcrd V(D)J recombination during T cell development. *J. Exp. Med.* 213:1921–1936. https://doi.org/10.1084/jem.20160670

Supplemental material

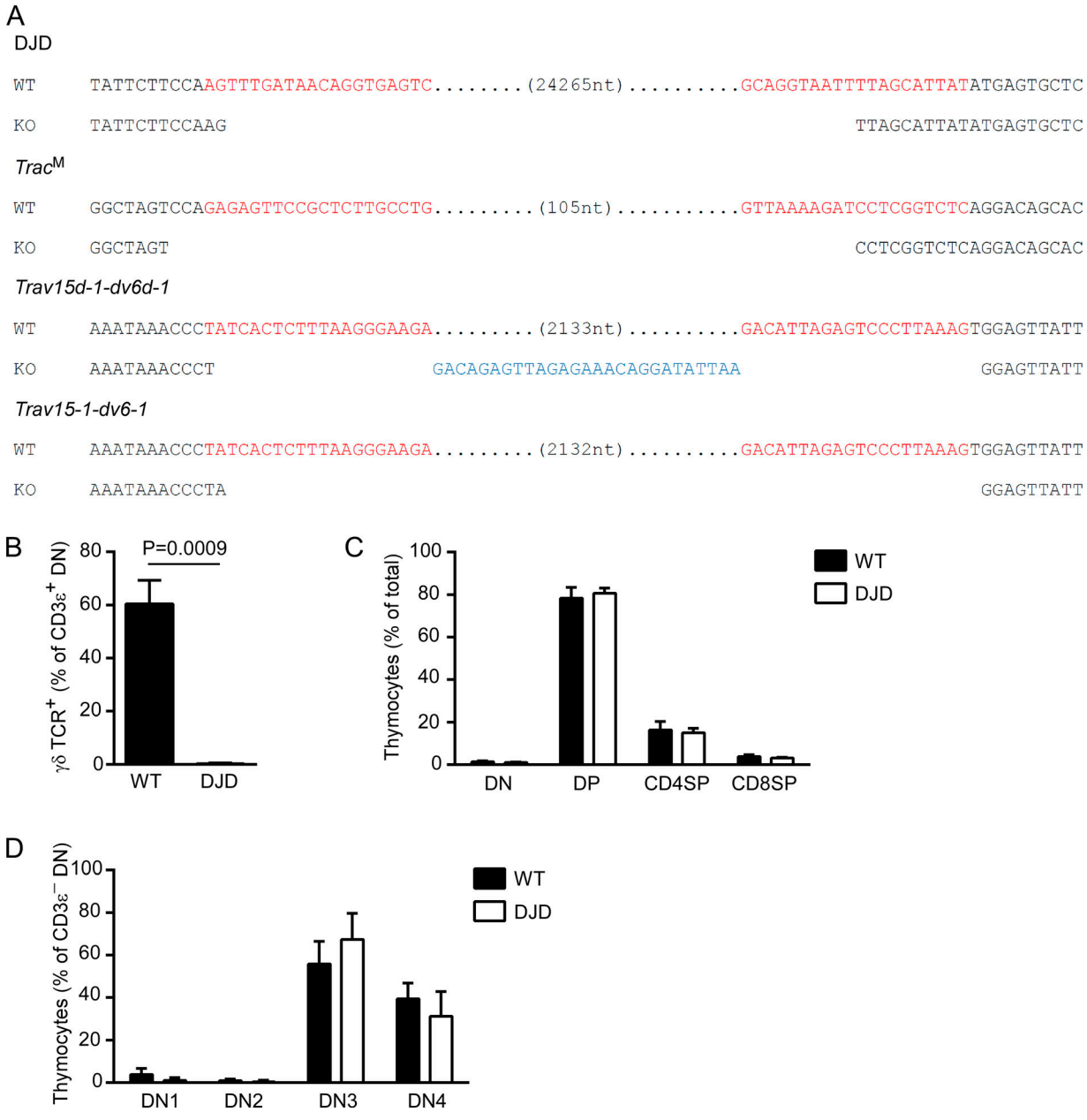

Figure S1. **Characterization of mutant mouse strains. (A)** DNA sequence of mutant alleles. Red, guide sequence for CRISPR/Cas9 targeting. Blue, nucleotides inserted in KO alleles. Gaps, nucleotides deleted in KO alleles. **(B–D)** Flow cytometric analysis of total thymocytes from WT and DJD littermate mice. Data are presented as mean and SD of four WT and five DJD littermates (mixed 129 and C57BL/6 background) analyzed in two independent experiments. Statistical significance was evaluated with unpaired *t* test with Welch's correction. Cells were pregated as 7-AAD$^-$CD11b$^-$CD11c$^-$Ter119$^-$B220$^-$Gr-1$^-$F4/80$^-$.

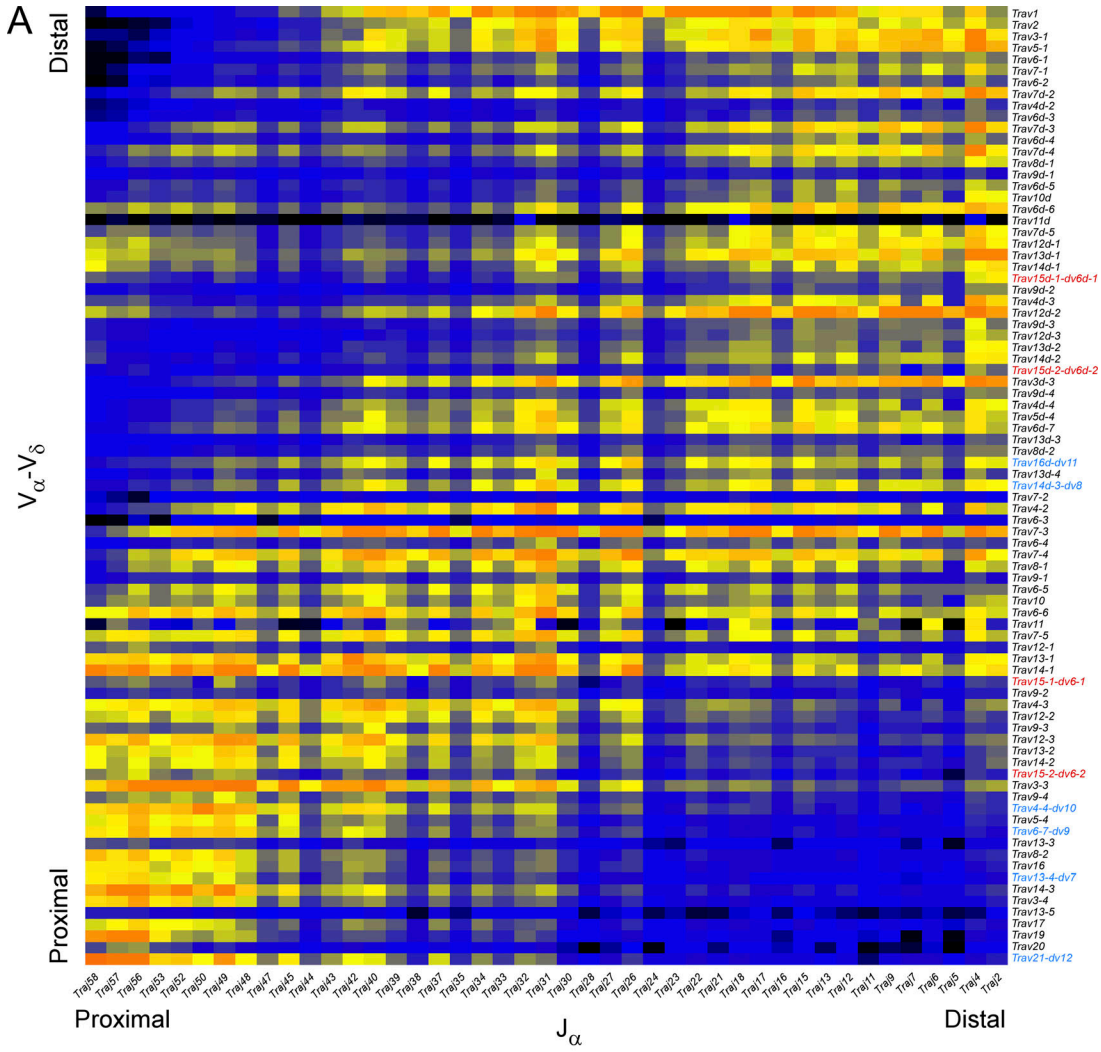

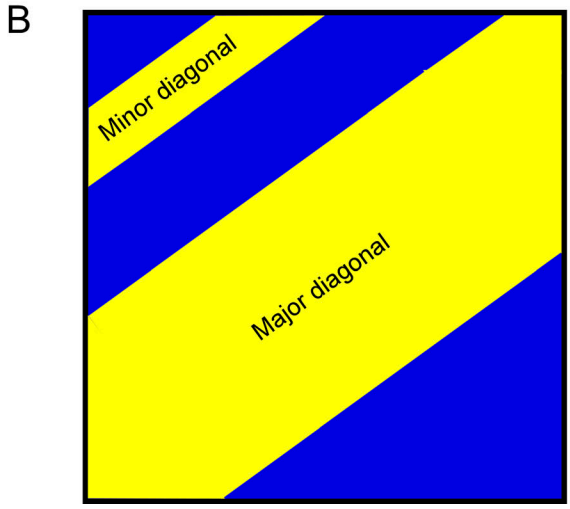

Figure S2. ***Tcra* repertoire in strain 129 preselection DP thymocytes. (A)** Average frequencies of V-J_α rearrangements in two WT strain 129 $CD4^+CD8^+CD3_\varepsilon^{lo}$ thymocytes (mixed 129 and C57BL/6 background; identical to Fig 1 B, left). Gene segment names are indicated on the right and lower margins. Red and blue lettering identifies Trav15-dv6 family V_δ segments and other V_δ segments, respectively. **(B)** Diagram indicating locations of major and minor diagonals in yellow, corresponding to the heatmap in A.

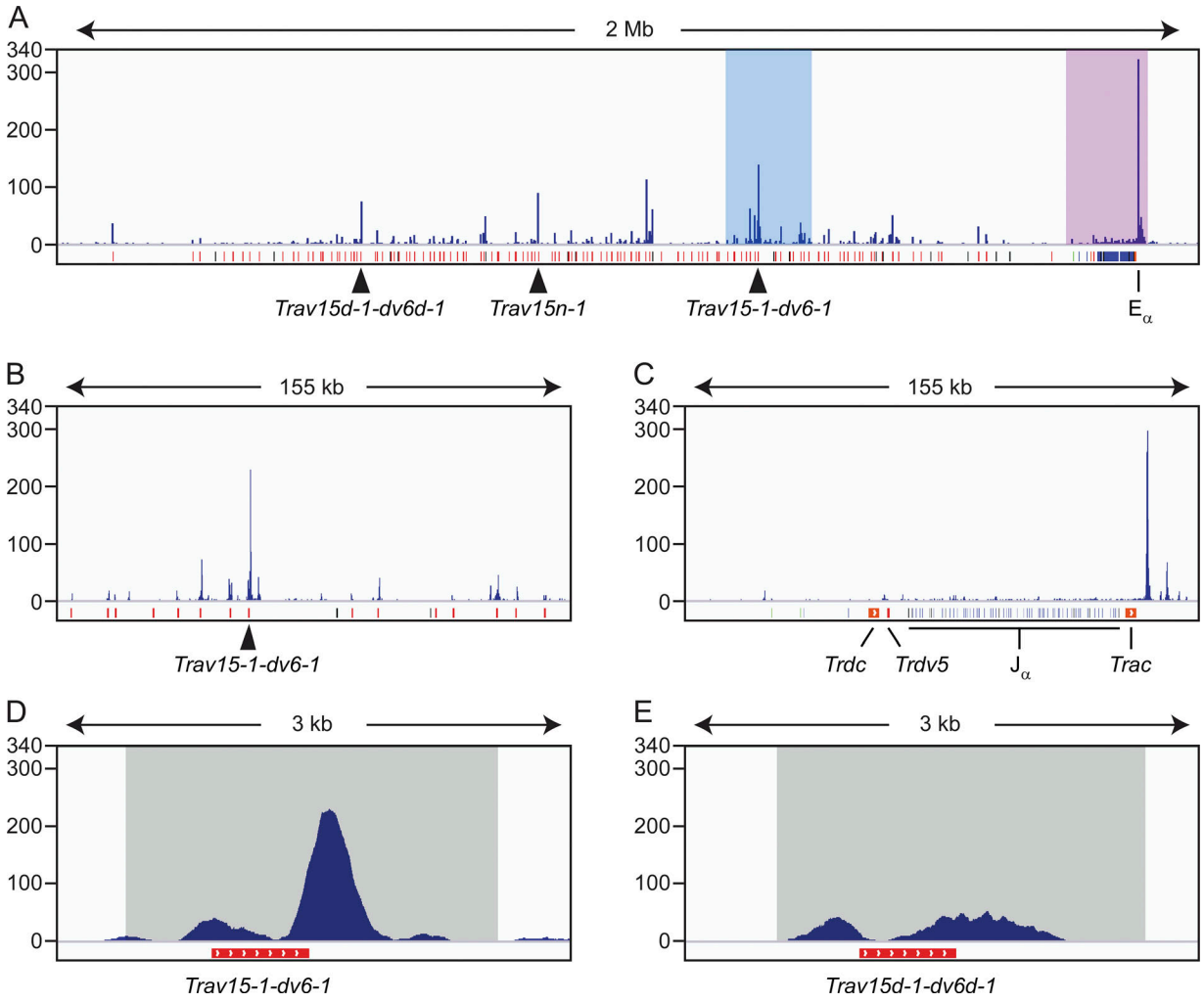

Figure S3. **E2A binding at the C57BL/6 *Tcra-Tcrd* locus.** Reanalysis of published E2A ChIP-seq data obtained from *Id2*- and *Id3*-deficient DP thymocytes (Roy et al., 2018). **(A)** E2A binding across the *Tcra-Tcrd* locus. V_α and V_δ (red bars), D_δ (green bars), J_α and J_δ (blue bars), and *Trdc* and *Trac* (orange bars) segments are indicated. Black bars represent pseudogenes. Compared with strain 129, the C57BL/6 *Tcra-Tcrd* locus contains an extra copy of several V_α segments, including *Trav15n-1*. **(B)** E2A binding across 155 kb surrounding *Trav15-1-dv6-1* (blue shaded region of A). **(C)** E2A binding across 155 kb encompassing *Trac* with major E2A peak at E_α (purple shaded region of A). **(D)** E2A binding at *Trav15-1-dv6-1*, with shaded region indicating the region of deletion on the $Tcrd^{CreER}$ allele (strain 129). **(E)** E2A binding at *Trav15d-1-dv6d-1*, with shaded region as in D.